Water Supply

IWA PUBLISHING

Water Supply Vol 21 No 8, 4514 doi: 10.2166/ws.2021.195

Ultrafiltration fouling behavior of natural organic matter: a perspective of EEM and molecular weight distribution

Gao Kuo [a,b] and Song Yuan [c,*]

[a] YANGTZE Eco-Environment Engineering Research Center, China Three Gorges Corporation, Shanghai 200335, China
[b] State Key Laboratory of Pollution Control and Resource Reuse, School of Environmental Science and Engineering, Tongji University, Shanghai 200092, China
[c] School of Economics and Management, Tongji University, Shanghai 200092, China
*Corresponding author. E-mail: 090121@tongji.edu.cn

GK, 0000-0002-5736-5399

ABSTRACT

As natural organic matter (NOM) can cause serious ultrafiltration (UF) membrane fouling, most previous studies on UF fouling caused by NOM focused on the contribution of NOM characteristics. In this study, the correlation of molecular weight and fluorescence characteristics was examined and the fouling behavior of NOM was examined in a comprehensive manner through a lot of analysis including redundancy analysis (RDA), parallel factor analysis (PARAFAC) and atomic force microscopy (AFM). The results showed that NOM from Tong Xin river was composed of humic acid (500 Da–8,000 Da), tryptophan-like substance, soluble microbial product (SMP) and aromatic protein (600,000 Da–2,000,000 Da). Notably, UF performance was significantly affected by the humic acid-like substance. Concurrently, the combined mechanism (CM) model was adopted to evaluate the fouling mechanism of NOM. The results indicated that the cake-intermediate model played an important part during membrane fouling and the cake layer fouling had a larger predominance over the intermediate blocking, which can be further proved in the membrane morphology detection.

Key words: EEM, molecular weight distribution, natural organic matter, RDA, ultrafiltration membrane fouling

HIGHLIGHTS

- The correlation of fractions with different molecular weight and fluorescent components was examined.
- Fouling potential of NOM fractions was ranked by RDA analysis.
- Humic acid like substance was the most detrimental foulant in the experiments.
- The cake-intermediate fouling played the domain part in UF fouling.

GRAPHICAL ABSTRACT

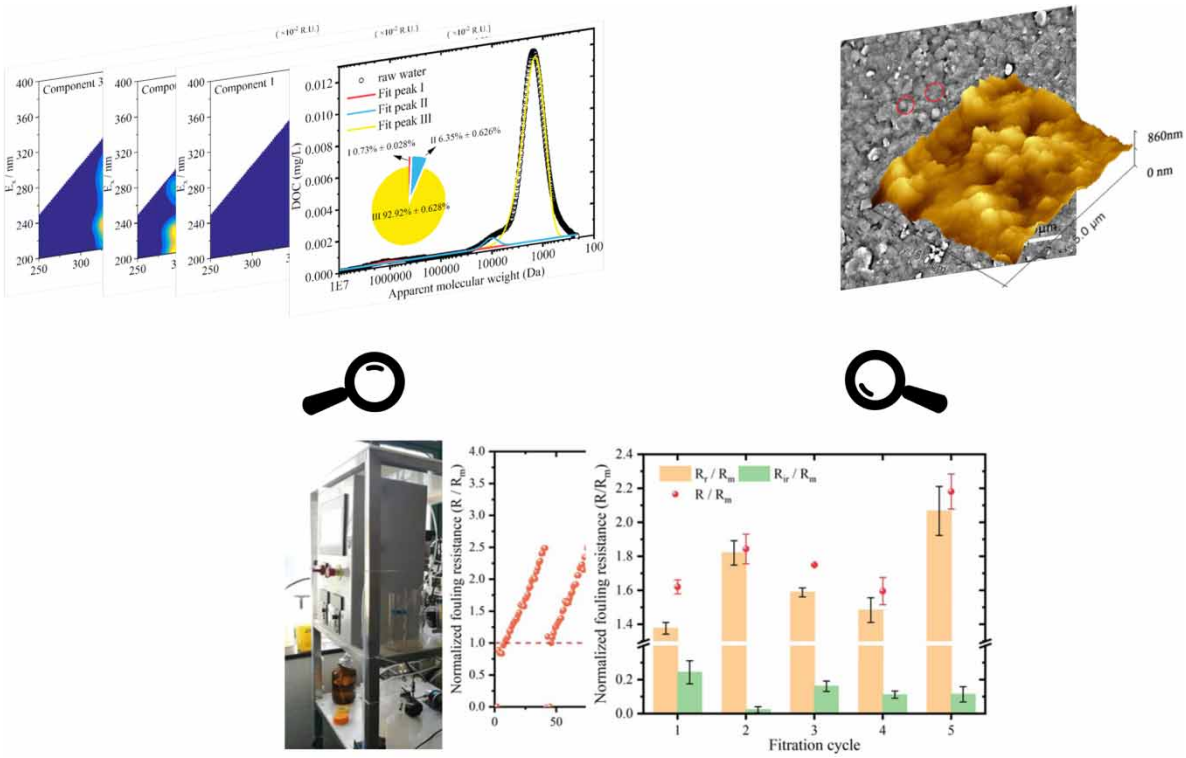

ABBREVIATIONS

NOM	natural organic matter
UF	ultrafiltration
RDA	redundancy analysis
PARAFAC	parallel factor analysis
AFM	atomic force microscope
SEM	scanning electron microscope
CM	combined mechanism
FEEM	fluorescence excitation emission matrix
EEM	excitation emission matrix
BP	biopolymers
SMP	soluble microbial product
HPSEC	high-pressure size exclusion chromatography
PLC	programmable logic controller
DOC	dissolved organic carbon
TOC	total organic carbon
UV_{254}	ultraviolet absorbance at 254 nm
AMWD	apparent molecular weight distribution

Subscripts

i intermediate blocking
c cake layer fouling

1. INTRODUCTION

NOM is a complex matrix of organic materials, and its amount, character, and properties vary considerably according to the origins of the waters and depend on the biogeochemical cycles of their surrounding environments (Sillanpää 2015).

Ultrafiltration (UF) is a promising technology to remove NOM with little chemical agent. However, the consequent membrane fouling has blocked the further application of UF to water treatment. Membrane fouling is the deposition of foulants on the membrane surface or in the pores, which results in the permeate flux decline or operational pressure increase. NOM is known as the most detrimental membrane foulant during water treatment (Shi *et al.* 2014; Wang *et al.* 2017b) and many studies have been focused on the contribution of NOM to membrane fouling till now (Kennedy *et al.* 2005).

Researchers have studied the influence of NOM characteristics (hydrophobicity/hydrophilicity, molecular weight, organic group, etc.) on membrane fouling. Chen Fei *et al.* conducted a pilot scale investigation of ultrafiltration for drinking water treatment between 2008–2010 and pointed out that the protein-like substances/biopolymers in NOM were major foulants during membrane fouling (Chen *et al.* 2014). Hiroshi Yamamura *et al.* put forward that the hydrophilic fraction resulted in severe fouling during ultrafiltration with the comparison of fouling difference between hydrophilic and hydrophobic fraction of NOM (Yamamura *et al.* 2014). In addition, contributions of fluorescent natural organic matter on membrane fouling were studied by Wang Hui *et al.* and fluorescent protein content played a key part in fouling layer formation (Wang *et al.* 2017a).

According to the mechanical sieving principle in low-pressure membranes, NOM fractions with greater molecular weight can block the membrane pores; while the fractions with relatively smaller molecular weight can enter the membrane pores interior. Thus, NOMs with different molecular weight fractions may have varied membrane fouling potential. Previous study showed that the high molecular weight fraction of NOM (>30 kDa) was responsible for the greater flux decline; for example, Kimura Katsuki et. al. pointed out that biopolymers (BP) with the molecular weight of >1 million Dalton had severe fouling potential for the large-size BP since they were not allowed to enter micro-pores. Lin *et al.* fractionated humic substances according to MW with gel permeation chromatography and hydrophobicity with resins. They found that the highest molecular weight (6.5–22.6 kDa) components for both hydrophobicity and hydrophilic fractions caused the greatest flux decline. Through examination of effects of molecular weight distribution of soluble microbial product (SMP) on membrane fouling, Teng Jiaheng *et al.* pointed out that the specific filtration resistance of SMP increased with molecular weight (Teng *et al.* 2020). However, through the filtration of different molecular fractions of HA, Li Chiwang *et al.* examined that the low molecular fraction (<3 kDa) caused the most severe membrane flux decline compared to other fractions, which they attributed to the interaction force between the molecules rather than the molecular weight (Li & Chen 2004).

These characteristics all have an impact on membrane fouling, but cannot give a good explanation of membrane fouling alone. Generally, membrane fouling is scarcely depicted by a single characteristic of NOM and combining the characteristics of NOM to give a comprehensive analysis is the feasible approach. The fouling behavior of NOM during UF was studied through advanced organic matter characterization methods including high-pressure size exclusion chromatography (HPSEC) and three-dimensional fluorescence spectroscopy coupled with parallel factor analysis (PARAFAC). In addition, the redundancy analysis (RDA) was also adopted to study the correlation between the removal of NOM fractions and membrane fouling resistance. Moreover, the combined mechanism (CM) model was used to evaluate the fouling mechanism of NOM fouling.

2. METHODS

2.1. Experimental setup

Dead-end filtration was adopted in the present study. The photos of the laboratory experimental setup are shown in Figure S1 (Supplementary Material). The experiments were carried out in a homemade membrane module at a temperature of 25°C ± 1°C, controlled by a water bath thermostat (DKB1915, JINGHONG, China). The feed water was driven through the membrane by a magnetic gear pump under a constant flux. The pressure and flow data were returned to a programmable logic controller (PLC) by a pressure transmitter (MIK-P300, Asmik, China) and flow transmitter (LSF38, OVAL, Japan) respectively every 1 minute.

The membrane module (Figure S1) was composed of a single membrane fiber (0.9 mm Multibore®, inge, GmbH, Germany) sealed in a polymethyl methacrylate tube with a mixture of polyurethane and epoxy resin. The modules had an effective membrane surface area of 39.6 cm^2. Before the filtration tests, pristine membrane modules were operated with Milli-Q water for 24 h to remove the organic residuals and wetting agents on the membranes and reached a constant operation pressure.

2.2. Feed water

The feed water for ultrafiltration experiments was collected from Tong Xin river in Tongji university. All samples were transported to the laboratory within 24 hours, then filtrated by 0.45 μm mixed cellulose ester filter (Xinya Co. Ltd, Shanghai,

China) and stored in a refrigerator at 4°. The dissolved organic carbon (DOC), ultraviolet absorbance (UV_{254}) and pH were measured immediately.

2.3. Ultrafiltration of NOM samples

The experiment procedure was controlled by a programmable logic controller (SIMATIC S7-1200, Siemens, Germany). The procedures and specific parameters were listed in Table 1.

The membrane performance was evaluated by the resistance-in-series model, which can be expressed as follows:

$$R_t = \frac{\Delta P}{\mu J} = R_m + R_{ir} + R_r \tag{1}$$

$$R_r = \frac{\Delta P_{n_t} - \Delta P_{(n+1)_0}}{\mu J} \tag{2}$$

$$R_{ir} = \frac{\Delta P_{(n+1)_0} - \Delta P_{n_0}}{\mu J} \tag{3}$$

where R_t, R_m, R_r and R_{ir} are the total resistance during the ultrafiltration (m^{-1}), the resistance of intrinsic membrane resistance (m^{-1}), hydraulic reversible resistance (m^{-1}) and hydraulic irreversible resistance (m^{-1}), respectively; μ is dynamic viscosity of the synthetic feed water (Pa·s); ΔP is the trans-membrane pressure (kPa); J the permeate flux during the ultrafiltration process (m/s) and the subscripts n, t, 0 are the filtration cycle number, end of every filtration cycle and initial stage of every filtration cycle, respectively. Notably, the average pressure value over 5 minutes is adopted as the calculated pressure to avoid sensor data deviation.

2.4. Analytical methods

The dissolve organic concentrations (DOC) were measured using a total organic carbon (TOC) analyzer (TOV-VCPH, Shimadzu, Japan). Ultraviolet light absorption at 254 nm was measured by a HACH UV-Vis spectrophotometer (DR5000, HACH, USA) and a 1 cm quartz cuvette. The molecular weight distribution of NOM was determined using a HPSEC method with a UV detector (UVA, Waters 2489) and on-line DOC detector (TOC, Sievers 900 Turbo TOC). Fluorescence excitation emission matrix spectra (FEEM) measurements were conducted using a Hitachi 7100 fluorescence spectrometer. The excitation and emission slits were set to 5.0 nm and excitation wavelengths were incrementally increased from 200 to 450 nm with a step of 10 nm. For each excitation wavelength, the emission wavelengths were detected at 2.0 nm gap from 275 to 575 nm.

PARAFAC was used to decompose the fluorescence components in the dataset of 36 EEMs of raw NOM samples. PARAFAC analysis was conducted using the DOMfluor toolbox (Stedmon *et al.* 2003) in Matlab® (version 2016, MathWorks Inc., Natick, MA).

The morphology of the membrane surface was obtained by SEM (Zeiss Sigma 300, Carl Zeiss Ltd, UK) and the surface roughness were analyzed using an atomic force microscope (AFM, FM-NanoviewOp-AFM). Fouled membranes (approximately 1 cm^2) were stuck to the magnetic stainless steel substrates and the surface was imaged at a scan size of 5 μm × 5 μm. AFM images were imported to the Gwyddion software to distinguish the height of samples by color scale, and then to calculate the surface roughness (Nečas & Klapetek 2012).

Table 1 | Parameters of ultrafiltration system operating conditions during a filtration cycle

Procedure	Flow (mL/min)	Duration (min)
Exhaust	16.0	1
Filtration[a]	8.0	40
Forward wash[b]	16.0	1
Backwash[b]	16.0	2

[a]The constant flux in this study was 120 L/(m^2 × h).
[b]The flow of forward wash and backwash were determined by manufacturer's recommendation.

3. RESULTS AND DISCUSSION

3.1. Fouling behavior during ultrafiltration

The normalized resistance variation during experiment was shown in Figure 1. The normalized total fouling resistances at the end of every cycle ranged from 2.5 to 4.0. The normalized hydraulic reversible resistance (R_r/R_m) and normalized irreversible resistance (R_{ir}/R_m) were calculated according to Equations (2) and (3), and results were shown in Figure 2, which is similar to the fouling behavior described by Maciej Szwast *et al.* (Szwast *et al.* 2013). Of note, R_r/R_m accounted for the main part of membrane fouling resistance. During the initial phase of filtration, R_{ir}/R_m experienced rapid growth for the mass organic colloidal adsorption. Subsequently, R_{ir}/R_m showed a dramatic decrease after initial adsorption, and gradually increased to around 0.1 R_m, which could be attributed to the pore blocking.

3.2. Molecular weight distribution of NOM

The apparent molecular weight distribution (AMWD) in NOM samples with the same DOC concentration (5.0 ± 0.1 mg/L) are shown in Figure 3. AMWD in different NOM samples can be divided into three regions, i.e. low molecular region III (500 Da–8,000 Da), medium molecular region II (5,000 Da–20,000 Da) and high molecular region I (600,000 Da–2,000,000 Da).

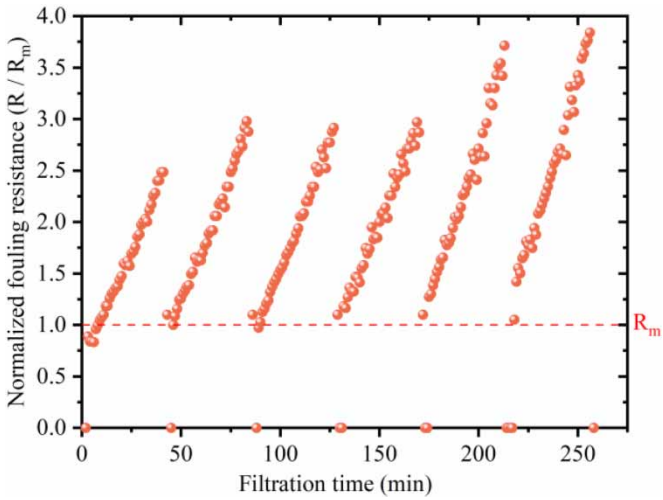

Figure 1 | Normalized resistance variation through filtration time.

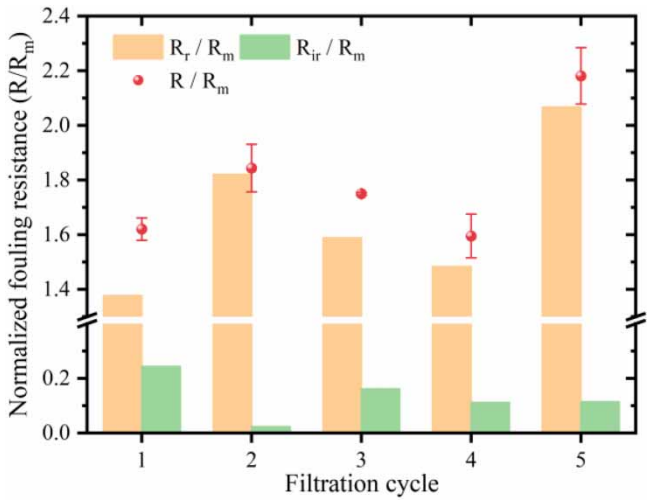

Figure 2 | Normalized fouling resistance during every filtration cycle.

A similar molecular weight distribution of NOM can be found in previous studies (Kennedy *et al.* 2005; Yamamura *et al.* 2007). Their proportions are 0.73% ± 0.028%, 6.35% ± 0.626% and 92.92 ± 0.628%, separately. Of note, organics in region I show a rare UV_{254} response, indicating the low aromatic structure of high molecular organics; organics in region II have the strongest UV_{254} response along with the moderate DOC response, and organics in region III account for most DOC response with lower UV_{254} response (Gao *et al.* 2021). It is thought that large molecules mainly consisted of polysaccharide or protein, whereas lower molecules mainly consisted of humic acid (Yamamura *et al.* 2007).

3.3. PAFARAC analysis

A total of 36 EEMs of NOM samples collected from Tong Xin river were used for PARAFAC analysis. According to the PARAFAC results, EEMs can be divided into three components as shown in Figure S2, which is consistent with NOMs from the previous studies (Table S1). Component 1 had an excitation peak at around 240 nm with an emission peak at around 430 nm. Furthermore, Component 1 was attributed to the humic acid component, indicating good matches with the published PARAFAC results (Chen *et al.* 2003; Senga *et al.* 2018). Component 2 had primary and secondary excitation peaks, occurring at around 200 nm–235 and 275 nm, respectively, and a single emission peak at around 300 nm. Component 2 was dominant in tryptophan-like substances, respectively, which differ in molecular weight and aromaticity. The prominent peak of Component 3 appeared at 225 nm/340 nm (E_x/E_m), linked to soluble microbial product (SMP) and aromatic protein fluorescence (Yamashita *et al.* 2010). Compared with Component 2, the blueshift of the EEM peak from 340 to 300 nm indicated a lower degree of condensation (Chen *et al.* 2003) and/or a lower molecular weight (Ishii & Boyer 2012).

3.4. Changes of EEM and molecular weight distribution

The maximum fluorescence intensity (F_{max}) was used to track changes of each component during UF; however, comparison between different components depends on the magnitude of their quantum efficiencies and their responses to quenching effects (Baghoth *et al.* 2011). Figure 4 shows the removal rate of F_{max} of each component in every filtration cycle. The F_{max} is determined by selecting the point of maximum intensity for each component in every sample (Vera *et al.* 2017). F_{max} of components 1 and 3 has a clear decline as the filtration cycle increased, and the F_{max} of component 2 did not show an obvious tendency. This is mainly because the fluorescence of Component 2 is related to the medium and low molecular organics (shown in Figure 6), which showed little removal.

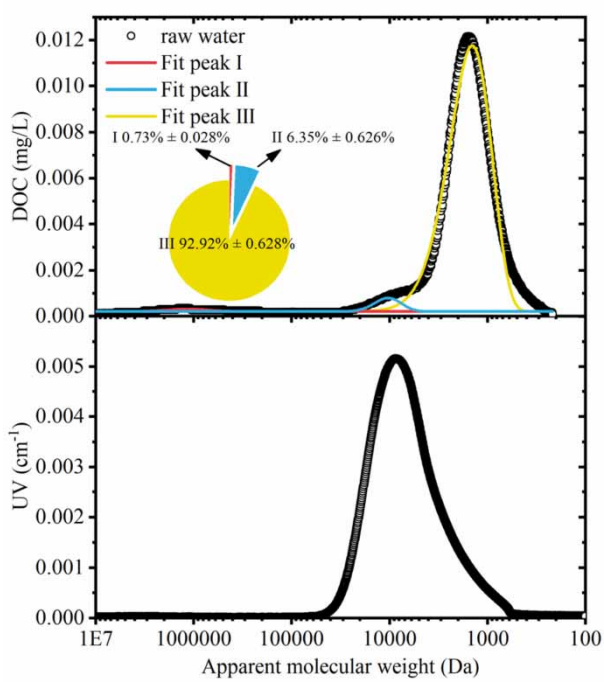

Figure 3 | Molecular weight distribution of NOM from Tong Xin river.

According to the AMWD of samples, the removal rate of different molecular weight (MW) fractions is shown in Figure 5. There was no significant difference between each filtration cycle in removal rates among each MW fraction besides fraction III. The removal rate of fraction III suffered a sharp decline and then slowly increased to a relatively stable value. That is mainly because of the rapid adsorption of low molecular organics in the initial phase and the retention capacity of the fouling layer in subsequent process.

3.5. Relation between fluorescent component and MW

The correlation between PARAFAC components and molecular weight regions is calculated by *R* (package *stats v4.0.2*) and the correlation heatmap is shown in Figure 6. The soluble microbial product and aromatic protein fluorescence (Component III) is significantly positively correlated with the high molecular region (Region I). That is, the soluble microbial product and aromatic protein in the feed water are mainly composed of high molecular organics (600,000 Da–2,000,000 Da). In addition, the humic acid component (Component 1) is significantly positively correlated with the low molecular region (Region III), which suggests that the humic acid in the feed water is mainly composed of low molecular organics (500 Da–8,000 Da).

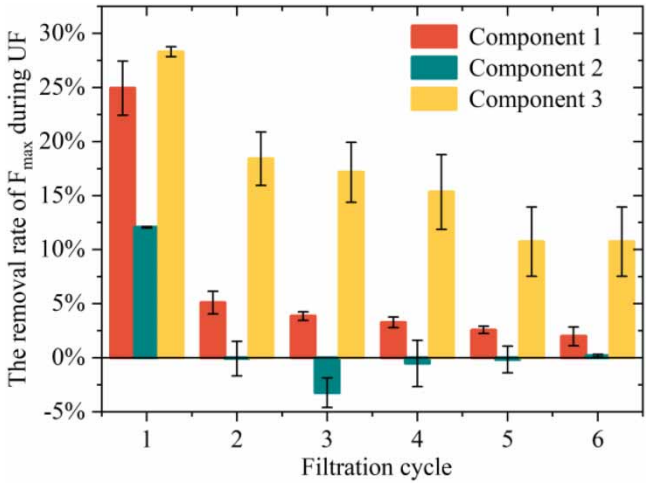

Figure 4 | Fluorescence maximum variation during ultrafiltration (values represent average ± standard deviation for two replicates).

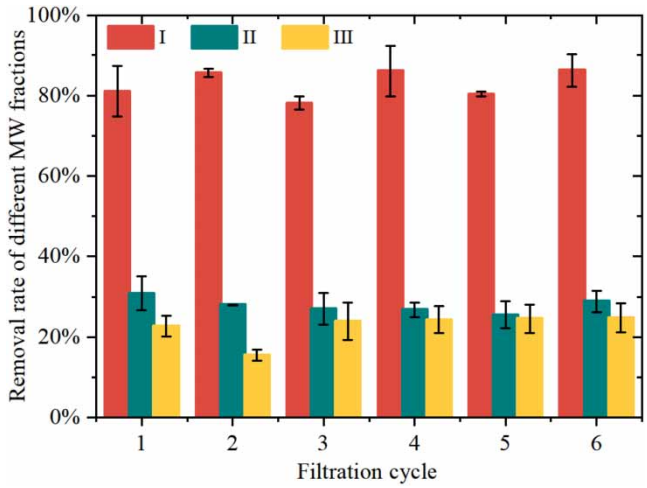

Figure 5 | Removal rate variation of different MW fractions during ultrafiltration (values represent average ± standard deviation for two replicates).

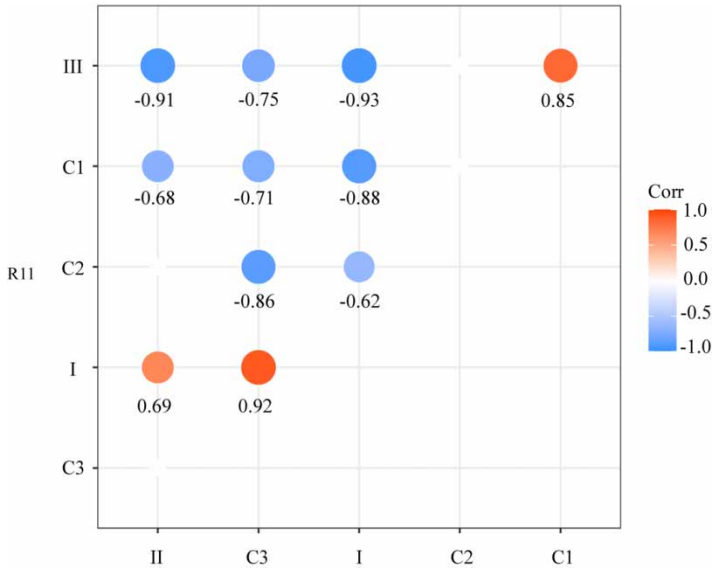

Figure 6 | The correlation heatmap between PARAFAC components and molecular weight regions (the data with p-value <0.05 are already hidden.).

3.6. Redundancy analysis between NOM properties and membrane fouling

Redundancy analysis (RDA) has been proved to be an effective multivariate statistical analysis method on the influence affecting membrane fouling (i.e., DOC, Zeta potential, metal ion concentration and so on) (Liu *et al.* 2019; Liu *et al.* 2020). Liu *et al.* analyzed the quantitative correlation between membrane fouling resistances and the influent characteristics by RDA during wastewater reclamation, and found that DOC, UV_{254} and protein were the most important positive factor in membrane resistance, and they verified the fouling alleviation effect of coupling ferrate pretreatment and in-situ ozonation (Liu *et al.* 2019). In the current study, RDA combined with the results of AMWD and PARAFAC was applied to further explore the specific correlation between the removal of different NOM fractions and membrane fouling resistances. As shown in Figure 7, axes 1 and 2 represent 71.93% and 19.77% of the total variance, respectively. Clearly, the removal of Components 1, I and III has positive correlation with normalized hydraulically reversible fouling resistance (R_r/R_m) and total fouling resistance (R_t/R_m). The contribution to R_r/R_m followed the sequence of the removal rate of Component 1 > I > III > Component 2–II, while the contribution to R_{ir}/R_m followed the sequence of the removal rate of II > Component 2 > III > I > Component 1. This can be due to the fouling resistance by Component 1 ($p = 0.05$**) and I ($p = 0.074$*) being 47.7% and 19.3%, which indicated they were the dominant factors in membrane fouling. In combination with the PARAFAC and AMWD results, humic acid-like, SMP and aromatic protein had highly positive correlation with R_{ir}/R_m, R_r/R_m and R_t/R_m.

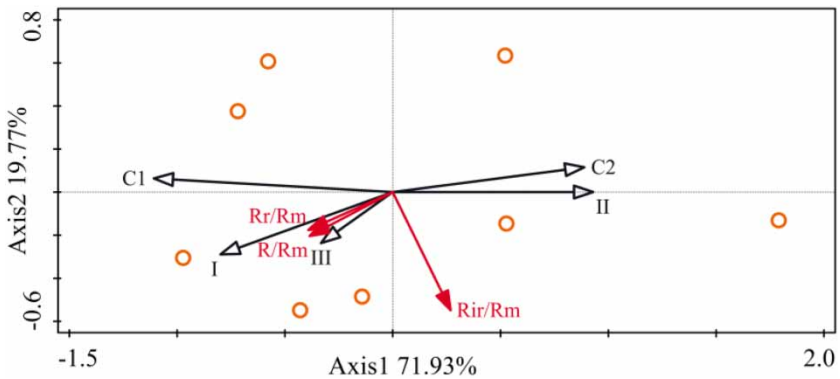

Figure 7 | Redundancy analysis on the correlation between the removal rate of NOM and membrane fouling resistances.

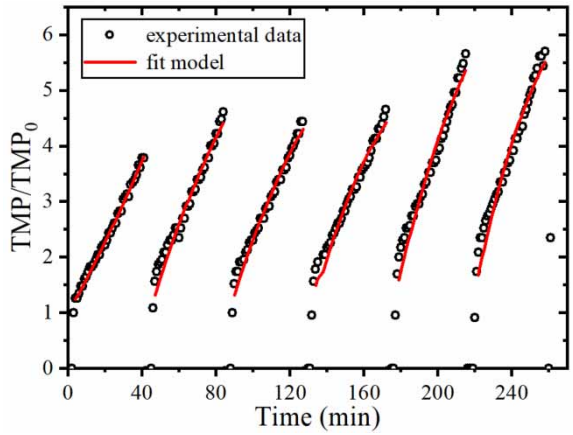

Figure 8 | Experimental data and combined model fit.

3.7. Fouling mechanism analysis

The combined mechanism model was used to analyze the fouling data. The model was described in detail in our previous study (Gao *et al.* 2021) and the fit result is presented in Figure 8 and Table 2. The cake-intermediate model exhibited higher R^2 than other blocking models. Since the terms K_i and K_cJ_0 have similar units (m^{-1}), the contributions of individual fouling mechanisms could be evaluated by comparison of their obtained fitted parameter values (Cerón-Vivas *et al.* 2018). Notably, the value of the ratio $|K_i/K_CJ_0|$ was 0.03–0.04 indicating that the cake layer fouling mechanism is dominant during the filtration and the morphology of the membrane surface also shows the existence of a dense cake layer (Figure S4).

3.8. Analysis of foulant layer morphology

The morphologies of the UF membranes used in the experiments are shown in Figure S3. There was a considerable difference between the pristine membrane and fouled membrane and the fouling layer can be easily observed on the membrane surface.

The surface morphology of fouled membranes was further detected by AFM. The three dimensional map visually displays undulation on the surface of the sample (Figure S4) and the surface parameters, the mean roughness (Sa) and the height of the foulant layer (h) are obtained by the Gwyddion software (Table 3). The surface of the pristine membrane showed a typical peak-to-valley structure, with Sa being 5.30 ± 0.12 nm. After being fouled by NOM, the membrane surface morphology

Table 2 | Results of the combined model

Fouling model	Filtration cycle	K_i	$K_c \times J_0$	$\frac{K_i}{K_c \times J_0}$	R^2
Cake-intermediate	1	94.78	157.41	0.04	0.9954
	2	−173.76	303.00	0.04	0.9708
	3	−197.23	416.55	0.03	0.9794
	4	−279.52	498.93	0.04	0.9729
	5	−230.92	557.69	0.03	0.9630
	6	−306.36	702.42	0.03	0.9631

Table 3 | The surface parameters of fouled membrane (provided by Gwyddion Rev 2.5.4)

	Mean roughness S_a (nm)	Average thickness of foulant layer h (nm)
Pristine membrane	5.3 ± 0.12	37.5 ± 5.78
Fouled membrane	87.6 ± 3.89	500.0 ± 10.90

varied significantly, attributed to the deposition of foulants. The Sa of the sample was 87.6 ± 3.89, and the h of samples increased to 37.5 ± 5.78 nm.

4. CONCLUSIONS

In this study, the fouling behavior of NOM was investigated by the fluorescent component and MW distribution. The primary conclusions were summarized as follows:

(1) Combined with the previous studies, PARAFAC results indicated that fluorescent NOM in feed water was mainly composed of humic acid, tryptophan-like substance, SMP and aromatic protein. The correlation analysis between PARAFAC components and molecular weight regions showed that the SMP and aromatic protein in feed water were mainly composed of high molecular organics (600,000 Da–2,000,000 Da) and the humic acid in the feed water was mainly composed of low molecular organics (500 Da–8,000 Da).
(2) The RDA results indicated that humic acid-like, SMP and aromatic protein had highly positive correlation with R_{ir}/R_m, R_r/R_m and R_t/R_m. That is, they were the dominant factors of membrane fouling.
(3) The fouling mechanism analysis indicated that the cake-intermediate model made a good description on the fouling behavior and the cake layer fouling had a larger predominance over the intermediate blocking on NOM fouling. Subsequently, the SEM and AFM images proved the existence of fouling layer.

ACKNOWLEDGEMENTS

The authors would greatly appreciate the financial support from the Major Science and Technology Program for Water Pollution Control and Treatment (No. 2017ZX07201001).

CONFLICT OF INTEREST

The authors have no conflicts to declare.

DATA AVAILABILITY STATEMENT

All relevant data are included in the paper or its Supplementary Information.

REFERENCES

Baghoth, S. A., Sharma, S. K. & Amy, G. L. 2011 Tracking natural organic matter (NOM) in a drinking water treatment plant using fluorescence excitation-emission matrices and PARAFAC. *Water Research* **45** (2), 797–809. doi:10.1016/j.watres.2010.09.005.

Cerón-Vivas, A., Kalboussi, N., Morgan-Sagastume, J. M., Harmand, J. & Noyola, A. 2018 Model assessment of the prevailing fouling mechanisms in a submerged membrane anaerobic reactor treating low-strength wastewater. *Bioresource Technology* **268**, 460–469. https://doi.org/10.1016/j.biortech.2018.08.017.

Chen, W., Westerhoff, P., Leenheer, J. A. & Booksh, K. 2003 Fluorescence excitation – emission matrix regional integration to quantify spectra for dissolved organic matter. *Environmental Science & Technology* **37** (24), 5701–5710. https://doi.org/10.1021/es034354c.

Chen, F., Peldszus, S., Peiris, R. H., Ruhl, A. S., Mehrez, R., Jekel, M., Legge, R. L. & Huck, P. M. 2014 Pilot-scale investigation of drinking water ultrafiltration membrane fouling rates using advanced data analysis techniques. *Water Research* **48**, 508–518. https://doi.org/10.1016/j.watres.2013.10.007.

Gao, K., Li, T., Zhao, Q., Liu, W., Liu, J., Song, Y., Chu, H. & Dong, B. 2021 UF fouling behavior of allelopathy of extracellular organic matter produced by mixed algae co-cultures. *Separation and Purification Technology* **261**, 118297. https://doi.org/10.1016/j.seppur.2020.118297.

Ishii, S. K. & Boyer, T. H. 2012 Behavior of reoccurring PARAFAC components in fluorescent dissolved organic matter in natural and engineered systems: a critical review. *Environ Sci Technol* **46** (4), 2006–2017. https://doi.org/10.1021/es2043504.

Kennedy, M. D., Chun, H. K., Quintanilla Yangali, V. A., Heijman, B. G. J. & Schippers, J. C. 2005 Natural organic matter (NOM) fouling of ultrafiltration membranes: fractionation of NOM in surface water and characterisation by LC-OCD. *Desalination* **178** (1), 73–83. https://doi.org/10.1016/j.desal.2005.02.004.

Li, C.-W. & Chen, Y.-S. 2004 Fouling of UF membrane by humic substance: effects of molecular weight and powder-activated carbon (PAC) pre-treatment. *Desalination* **170** (1), 59–67. https://doi.org/10.1016/j.desal.2004.03.015.

Liu, J., He, K., Zhang, J., Li, C. & Zhang, Z. 2019 Coupling ferrate pretreatment and in-situ ozonation/ceramic membrane filtration for wastewater reclamation: water quality and membrane fouling. *Journal of Membrane Science* **590**, 117310. https://doi.org/10.1016/j.memsci.2019.117310.

Liu, Z., Yu, J., Xiao, K., Chen, C., Ma, H., Liang, P., Zhang, X. & Huang, X. 2020 Quantitative relationships for the impact of gas sparging conditions on membrane fouling in anaerobic membrane bioreactor. *Journal of Cleaner Production* **276**, 123139. https://doi.org/10.1016/j.jclepro.2020.123139.

Nečas, D. & Klapetek, P. 2012 Gwyddion: an open-source software for SPM data analysis. *Central European Journal of Physics* **10** (1), 181–188. https://doi.org/10.2478/s11534-011-0096-2.

Senga, Y., Yabe, S., Nakamura, T. & Kagami, M. 2018 Influence of parasitic chytrids on the quantity and quality of algal dissolved organic matter (AOM). *Water Research* **145**, 346–353. https://doi.org/10.1016/j.watres.2018.08.037.

Shi, X., Tal, G., Hankins, N. P. & Gitis, V. 2014 Fouling and cleaning of ultrafiltration membranes: a review. *Journal of Water Process Engineering* **1**, 121–138. https://doi.org/10.1016/j.jwpe.2014.04.003.

Sillanpää, M. 2015 *Natural Organic Matter in Water* (Sillanpää, M., ed.). Butterworth-Heinemann, Oxford, UK, pp. 1–15.

Stedmon, C. A., Markager, S. & Bro, R. 2003 Tracing dissolved organic matter in aquatic environments using a new approach to fluorescence spectroscopy. *Marine Chemistry* **82** (3), 239–254. https://doi.org/10.1016/S0304-4203(03)00072-0.

Szwast, Z., Szwast, M., Grądkowski, M. & Piątkiewicz, W. 2013 Modelling of postproduction suspensions' concentration processes by 'Batch' membrane microfiltration. *Chemical and Process Engineering* **34** (3), 313–325.

Teng, J., Shen, L., Xu, Y., Chen, Y., Wu, X.-L., He, Y., Chen, J. & Lin, H. 2020 Effects of molecular weight distribution of soluble microbial products (SMPs) on membrane fouling in a membrane bioreactor (MBR): novel mechanistic insights. *Chemosphere* **248**, 126013. https://doi.org/10.1016/j.chemosphere.2020.126013.

Vera, M., Martín-Alonso, J., Mesa, J., Granados, M., Beltran, J. L., Casas, S., Gibert, O. & Cortina, J. L. 2017 Monitoring UF membrane performance treating surface-groundwater blends: limitations of FEEM-PARAFAC on the assessment of the organic matter role. *Chemical Engineering Journal* **317**, 961–971. https://doi.org/10.1016/j.cej.2017.02.081.

Wang, H., Ding, A., Gan, Z., Qu, F., Cheng, X., Bai, L., Guo, S., Li, G. & Liang, H. 2017a Fluorescent natural organic matter responsible for ultrafiltration membrane fouling: fate, contributions and fouling mechanisms. *Chemosphere* **182**, 183–193. https://doi.org/10.1016/j.chemosphere.2017.04.148.

Wang, H., Park, M., Liang, H., Wu, S., Lopez, I. J., Ji, W., Li, G. & Snyder, S. A. 2017b Reducing ultrafiltration membrane fouling during potable water reuse using pre-ozonation. *Water Research* **125**, 42–51. https://doi.org/10.1016/j.watres.2017.08.030.

Yamamura, H., Kimura, K. & Watanabe, Y. 2007 Mechanism involved in the evolution of physically irreversible fouling in microfiltration and ultrafiltration membranes used for drinking water treatment. *Environmental Science & Technology* **41** (19), 6789–6794. doi:10.1021/es0629054.

Yamamura, H., Okimoto, K., Kimura, K. & Watanabe, Y. 2014 Hydrophilic fraction of natural organic matter causing irreversible fouling of microfiltration and ultrafiltration membranes. *Water Research* **54**, 123–136. https://doi.org/10.1016/j.watres.2014.01.024.

Yamashita, Y., Scinto, L. J., Maie, N. & Jaffé, R. 2010 Dissolved organic matter characteristics across a subtropical wetland's landscape: application of optical properties in the assessment of environmental dynamics. *Ecosystems* **13** (7), 1006–1019. doi:10.1007/s10021-010-9370-1.

First received 18 April 2021; accepted in revised form 11 June 2021. Available online 24 June 2021